J of Nuclear Medicine Technology, first published online April 24, 2019 as doi:10.2967/jnmt.118.221317

Automated quantitative analysis of ACR PET phantom images

Frank P. DiFilippo[1], Meghal Patel[1], and Sagar Patel[1]

[1]Department of Nuclear Medicine, Cleveland Clinic, Cleveland, OH 44195 USA

Address for Correspondence:

Frank P. DiFilippo, PhD
Dept. of Nuclear Medicine
Cleveland Clinic
9500 Euclid Avenue / Jb3
Cleveland, OH 44195

Phone: 216-445-9378
FAX: 216-444-3943
e-mail address: difilif@ccf.org

Short title: ACR PET phantom automated analysis

Word count: 4,416

Submit to: *J Nucl Med Technol*

Abstract:

Evaluation of PET image quality is central to annual physics surveys, quality assurance, and laboratory accreditation. A common method is to image the American College of Radiology (ACR) PET phantom, which contains hot and cold structures of various sizes in a warm background. Performance evaluation involves qualitative assessment of hot and cold structure visibility and overall image quality. Some criteria are quantitative and rely on manually-drawn regions of interest (ROIs) to measure standardized uptake value (SUV). Fully automated scoring of ACR PET phantom images would improve efficiency, avoid observer-related dependencies, and may provide more robust evaluation of image quality.

Methods: Software was developed to co-register PET images to a phantom template and to compute ROI measurements of hot vial activity (SUV-max) and background activity (SUV-mean) automatically. In addition, three-dimensional volumes of interest (VOIs) were generated to measure hot vial activity ("SUV-vial"), background activity, and cold rods contrast. Consistency of the ROI-based and VOI-based methods was evaluated using phantom data from a total of 17 annual physics surveys of three PET/CT scanners with the same PET detector designs.

Results: The automated software processed all PET phantom datasets successfully. SUV consistency for hot vials was improved through use of cylindrical VOIs and through normalization with respect to assayed activities and dilution volumes used in phantom preparation. Average vial SUV standard deviation improved from 8.0% for standard SUV-max to 3.2% for normalized SUV-vial. Similarly, standard deviation for SUV ratio of 16mm to 25mm vials improved from 5.0% for SUV-max to 3.2% for SUV-vial. Background mean SUV had similar consistency between the ROI and VOI methods. Cold rods contrast was highly consistent, offering a potential alternative to qualitative visual assessment of low-contrast performance.

Conclusion: Automated quantitative scoring of the ACR PET phantom is feasible and offers advantages of more efficient, consistent, and thorough performance characterization. Acceptance ranges for SUV values and ratios likely can be tightened if normalized VOI measurements are used. Further testing with phantom data from a variety of PET scanners is necessary to establish suitable quantitative thresholds for acceptable performance.

Key Words: PET, ACR phantom, quality assurance, quantitative

Introduction

Evaluation of positron emission tomography (PET) image quality is a component of laboratory accreditation, annual physics surveys, and routine quality assurance. The American College of Radiology (ACR) PET phantom is commonly used for this purpose (*1*). The ACR PET phantom consists of a 20-cm cylinder with six sectors of cold rods (12.7, 11.1, 9.5, 7.9, 6.4, and 4.8 mm diameters) and a lid with four hot vials (25, 16, 12, and 8 mm diameters) and three cold vials/cylinders (25 mm diameter) representing bone, air, and water. The hot vials and warm background chamber are filled with ^{18}F solutions, prepared by drawing syringes of prescribed activity (±10%) and by diluting to 2.4:1 activity concentration ratio. The phantom is scanned using the laboratory's typical wholebody imaging protocol, starting 60 minutes after assaying the syringes in a dose calibrator.

Evaluation of ACR PET phantom images involves three steps (*2*). First, the reconstructed PET images are reformatted as a series of transaxial images of 10-mm slice thickness. Second, the images are evaluated qualitatively in regards to visibility of the hot vials and cold rods and uniformity of the background region. Third, region-of-interest (ROI) measurements are made in a single 10-mm-thick slice through the hot and cold vials to measure standardized uptake value (SUV) of each vial and the central background region (Figure 1).

When applying to ACR for accreditation, phantom images must be submitted: a complete montage of slices, and a slice through the vials showing the ROIs and SUV measurements. In order to be acceptable, the phantom study must demonstrate all of the following (*2*):

- Maximum SUV of 25-mm hot vial: between 1.8 and 2.8
- Ratio of (SUV-max-16mm vial) / (SUV-max-25mm vial): at least 0.7
- Mean SUV of background region: between 0.85 and 1.15
- Visual assessment of hot vials: 12 mm vial is visualized with low contrast; larger vials resolved with high contrast
- Visual assessment of cold rods: 9.5 mm rods visualized with low contrast; larger rods are resolved with high contrast
- Visual assessment of uniformity: Artifacts are seen in only a few slices of the complete set but are not thought to be clinically significant

Qualitative assessment of image quality is performed by two trained physicist reviewers.

Several groups have developed automated software for computing quantitative measurements of PET and single photon emission computed tomography (SPECT) phantom studies (*3-8*). Automated quantitative analysis is desirable for reasons besides saving time and effort associated with manual drawing of ROIs and calculations. Visual assessment of phantom image quality relies on verbal scoring criteria that might be perceived differently by individuals. Manual image-based measurements, though quantitative, also have limited repeatability and are suitable only for simple metrics. By implementing more complex algorithms without user interaction, automated software is expected to avoid inter-observer and intra-observer variability

and to potentially allow for more consistent and meaningful assessment of image quality. Robust measures are necessary for monitoring changes in scanner performance in annual physics surveys and for harmonizing image quality in multi-center clinical trials (*9*).

Towards the goal of robust assessment of PET performance, software was developed to perform automated quantitative measurements from PET images of the ACR phantom for evaluation of image quality. In addition to measuring the standard single-slice ROIs specified by ACR, additional three-dimensional (3D) volume-of-interest (VOI) measurements were made to evaluate high-contrast performance, low-contrast performance, and uniformity. Reliability of these measurements was assessed and compared by retrospective analysis of images acquired during PET annual physics surveys of scanners having similar PET detector designs spanning multiple years.

Materials and Methods:

Software was developed in C#/C++ (Visual Studio Express, Microsoft) along with the open-source gdcm library (*10*) for Digital Imaging and Communications in Medicine (DICOM) files to perform the multiple steps associated with data analysis, as follows:

1. Template generation: The first step was to compute digital template images of the phantom based on its known geometry, as determined from mechanical drawings provided by the manufacturer. This task was complicated by the fact that the phantom may be assembled in various configurations. The cold rods insert may be attached so that the rods are increasing in diameter in a clockwise or counter-clockwise direction, and the lid with fixed hot and cold vials may be attached in six possible orientations at 60° intervals. For each possible configuration, a template image was generated with the phantom centered in a 256-mm cubic volume with 192x192x192 sampling (voxel size = 1.333 mm). These template images were pre-computed using linear interpolation and stored to disk.

2. Data input interface: The user interface allowed the user to identify the DICOM images to be processed. The DICOM headers provided most parameters needed to process images and to compute SUV. The user also entered the necessary data associated with phantom preparation (syringe activities, residual activities, assay times, and type of dilution vessel).

3. PET Pre-Processing: After reading DICOM data and generating SUV volume images, the scan configuration was determined. The PET slices were analyzed to determine whether the phantom had been positioned with the vials' side or the rods' side facing the gantry. The slices were then analyzed to determine the actual phantom configuration (cold rods orientation, and lid attachment angle).

4. Co-registration: The PET image volume was co-registered to the template matching the scan configuration as determined in the prior step, using the mutual information algorithm with 256 gray levels, with linear interpolation, and without landmarks (*11,12*). For analysis of low contrast performance (step 7, below), a separate co-registration was performed using a template only having cold rods, to allow for potential variability in the attachment of the cold rods insert to the

phantom body. The PET data were resampled to match the template voxels by linear interpolation.

5. Standard ACR measurements: Slices of 10-mm thickness were generated, as specified by ACR. The standard ROIs were placed on the central slice through the vials to obtain SUV measurements. The background activity concentration was measured as the SUV-mean of a 70-mm diameter circle centered on this slice. The hot vials were characterized by the SUV-max of 25-mm diameter circles centered on each hot vial of this slice.

6. High-contrast performance: In addition to the single-slice measurements specified by ACR, the hot vials were characterized using 3D VOIs. For each hot vial, a cylindrical VOI of height 30 mm and of diameter half that of the vial was centered in the vial. The mean SUV of this cylindrical VOI, designated as "SUV-vial", reflected the contrast recovery performance for each hot vial.

7. Low-contrast performance: The cold rods portion of the phantom characterized the low contrast performance of the PET scanner. For each of the six sectors of the cold rods pattern, cylindrical VOIs were positioned on the centers of the cold rods and on the midpoints between adjacent cold rods. The VOI diameter was half the cold rod diameter, and the VOI height was 80 mm. The contrast for each sector was calculated as the difference of the mean midpoint VOI activity and the mean cold rods VOI activity, divided by the mean midpoint VOI activity.

8. Background (SUV accuracy and noise): A 3D VOI was generated encompassing the entire background region of the phantom while avoiding edge effects. This VOI included all voxels in the upper portion of the phantom, except those within 12 mm of the outer wall, lid, vials, or cold rods insert. The mean SUV and standard deviation were computed for voxels within this VOI.

Processing time per PET phantom dataset was approximately one minute, using a Dell T5400 workstation with dual Intel Xeon E5405 2.0 GHz quad-core processors.

The software was run retrospectively on PET phantom images from a total of 17 prior annual physics surveys of three PET/CT scanners with the same detector designs (Siemens Biograph mCT, with time-of-flight capability). Images had been acquired at two bed positions for 3 minutes per bed position, starting 60 minutes after assaying the syringes prepared with ^{18}F solution. All images had been reconstructed with the same parameters: iterative time-of-flight algorithm with resolution modeling ("Ultra-HDPET"), 2 iterations, 21 subsets, 4 mm post-filter.

In each case, the phantom had been prepared according to ACR's instructions, using a reference patient dose of 370 MBq (10 mCi) (*2*). All relevant details of phantom preparation had been recorded, including assayed activities of the syringes added to the dilution vessel used for the vials ("Dose A") and to the background chamber ("Dose B"), along with their residual activities and assay times. Syringe minus residual activities (mean ± standard deviation) for Dose A and Dose B were 12.9 ± 0.3 MBq (350 ± 7 μCi) and 30.7 ± 0.2 MBq (829 ± 5 μCi), respectively. The dilution vessel was either a 1-liter saline bag or a plastic bottle filled with 1 liter of water measured with a volumetric flask.

SUVs were calculated based on a patient weight of 70 kg, an injected activity of 370 MBq, the syringe assay times, and the actual scan start time. In addition, "normalized SUVs" were calculated to account for the measured syringe activities (and residual activities) and the volume of the dilution vessel used in phantom preparation. The actual volumes of the 1-liter saline bags were not measured, though it has been reported that a sample of 1-liter saline bags had an average volume of 1051 mL (range 1033-1069 mL) (*13*). Thus the software assumed a dilution volume of 1.05 L when calculating the hot vial's normalized SUVs for phantoms prepared using 1-liter saline bags.

Results:

Hot vial SUV measurements:

Measurements of hot vial SUVs and normalized SUVs calculated according to the ACR guidelines (SUV-max) and using the cylindrical VOIs (SUV-vial) are listed in Table 1. For all vial diameters, the SUV-vial measurements based on the cylindrical 3D VOIs had higher consistency across the 17 phantom datasets, compared to the standard SUV-max measurements. Consistency in SUV-max and SUV-vial measurements was improved further through normalization with respect to assayed syringe activities and dilution vessel volume. Starting with the established ACR procedure, the percent standard deviation for SUV-max averaged 8.0% for the vials. By accounting for activities and volumes, the average percent standard deviation improved to 5.5% for normalized SUV-max and, by using cylindrical VOIs, further improved to 3.2% for normalized SUV-vial.

Histograms of measurements for the 16 mm vial are presented in Figure 2. Compared to ACR SUV-max measurements, the SUV-vial measurements were more consistent and had fewer outliers. Normalization noticeably improved consistency in both cases, and best results were obtained with the normalized SUV-vial measurements.

Hot vial SUV ratios:

Measurements of the SUV-max ratio and the SUV-vial ratio for the hot vials are listed in Table 2. (Note that the effects of normalization cancel in the ratio calculation, thus the ratios of normalized SUV are redundant.) In all cases, the SUV-vial ratios based on cylindrical VOIs were more consistent than the SUV-max ratios from single-slice ROIs. The SUV ratio of 16 mm to 25 mm vials is of particular interest, since ACR sets quantitative acceptance limits for this ratio to evaluate contrast recovery performance (*2*). Histograms of the SUV-max ratio and the SUV-vial ratio for the 16 mm to 25 mm hot vials are shown in Figure 3. The percent standard deviation for the 16 mm to 25 mm hot vial ratio improved from 5.0% for SUV-max ratio to 2.7% for SUV-vial ratio. In addition, the SUV-max ratio had outliers exceeding 1.0, which is inconsistent with the partial volume effect.

Background (SUV accuracy and noise):

Background SUV-mean was 1.008 ± 5.2% (mean ± percent standard deviation) as measured by the ACR circular ROI and was 1.012 ± 5.6% as measured by the automated 3D VOI. Both the means and standard deviations were in agreement between the two methods. Noise in the background region, measured as the standard deviation of voxel SUVs in the 3D VOI divided by the mean, averaged 6.8%.

Cold rods contrast:

Cold rods contrast measurements (mean and standard deviation, for the 17 phantom studies) are listed in Table 3 and graphed in Figure 4. Contrast was greater than 0.2 for the largest four sectors of cold rods, which were visually resolved in the 10 mm image slices. (For reference, ACR's acceptance criterion for cold rods visibility is that the third-largest sector be resolved with low contrast and that larger rods be resolved with high contrast (*2*).)

Discussion:

The automated software ran successfully in all cases and was more efficient than manual processing using an image workstation. The software succeeded in determining the actual phantom configuration from the PET images and in co-registering the images to the correct digital phantom template. Although CT images could have been used instead of a digital template, image analysis would have been subject to errors associated with noise and possible artifacts. A goal of the automated software was to enable new measurements based on 3D VOIs for more meaningful quantitative evaluation of PET performance. The availability of 17 prior phantom studies acquired with scanners having the same PET detector designs provided an opportunity to evaluate the consistency of the VOI-based measures versus the standard single-slice ACR measures.

Under the ACR procedure, high-contrast performance is assessed quantitatively by SUV-max of the 25 mm hot vial, which must be in the range of 1.8 to 2.8. This represents a rather large acceptance range that is ±22% with respect to the central value and indicates the large variability in SUV-max results obtained from typical phantom scans. As known in oncologic PET studies, SUV-max is subject to noise, especially when using iterative reconstruction algorithms with high number of iterations (*14,15*). Ringing artifacts, which can occur when including resolution modeling during image reconstruction, also can artificially increase SUV-max (*16*). SUV-peak, which is the maximum value of SUV averaged over a specified VOI (10-mm diameter sphere, typically), often is used instead of SUV-max to characterize lesion uptake due to its reduced sensitivity to noise (*17,18*). Similarly, the SUV-vial measurements using cylindrical VOIs were expected to yield more consistent assessment of vial activity concentration, as was confirmed by the phantom data. Consistency of vial SUV measurements was improved further by normalizing with respect to measured activities of syringes used during phantom preparation and to dilution vessel volume. In these phantom studies, the syringe doses had been prepared carefully to closely match the specified activities (standard deviation = 2%). Even so, this variance contributed to non-normalized SUV variance.

Contrast recovery performance is assessed quantitatively by the SUV ratio of the 16 mm to 25 mm hot vials, which according to ACR must be greater than 0.7. Fortunately, actual doses and volumes associated with preparing the phantom cancel in the ratio calculation. However, error associated with SUV measurements contributes twice in the ratio calculation, which is a concern. The consistency of the SUV-max ratio was limited, as seen in Figure 3, and occasionally a ratio larger than 1.0 was obtained. The SUV-vial ratio was more consistent, with measurements clustered tightly around a mean of 0.91. Although in all cases the results passed the ACR criterion, the improved accuracy with the SUV-vial ratio has benefits for detecting changes in scanner performance in annual surveys.

SUV accuracy evaluated according to SUV-mean of the ACR single-slice ROI had consistency similar to SUV-mean of the background 3D VOI. This indicates that in these phantom studies, mean SUV measured by a 70-mm diameter circular ROI in a single 10-mm slice was representative of the entire background volume. However, it is likely that a scanner with an outdated normalization calibration would exhibit non-uniformity across slices and would be better characterized by the 3D VOI SUV-mean and statistical distribution.

Low-contrast performance is evaluated qualitatively in the ACR protocol, by identifying the number of cold rods sectors that are visually resolved. Quantitative evaluation of cold rods contrast with the automated software offers a more meaningful assessment of low-contrast performance, provided that the measurement has high reproducibility. In these phantom studies, cold rods contrast measurements by the automated algorithm were highly consistent, varying by approximately 0.01. This result indicates that low-contrast performance can be compared precisely between time-points or scanners and that variance associated with algorithm implementation and image registration was small. Since the contrast versus rod diameter curve is smooth with small errors, the curve may be interpolated to determine a minimum detectable rod diameter corresponding to a specified threshold (*19*).

Overall, the automated software enables reliable quantitative evaluation of PET scanner performance with the ACR phantom. In addition to the improved consistency associated with the use of 3D VOIs (SUV-vial instead of SUV-max), further improvement was achieved by normalizing measurements to assayed activities and to dilution vessel volume. ACR's current quantitative pass/fail criteria are rather broad (±22% for vial SUV, and ±15% for background SUV), apparently to account for variance in phantom preparation and for noise associated with single-slice SUV-max measurement. By compensating for these sources of error, normalized SUV-vial measurements may allow the acceptance ranges to be tightened. Note that if tighter acceptance ranges are implemented, dose calibrator accuracy may become a factor. In recent years, the recommended dose calibrator dial settings have changed more than once, by several percent (*20,21*). SUV measurements are affected by dose calibrator settings unless cross-calibration is performed routinely.

Although the use of automated software is promising, this study had limitations which require further investigation. Data were studied from only one PET detector design and one set of reconstruction parameters. This approach allowed for evaluation of the consistency of the automated analysis over a group of similar PET studies, but it did not characterize differences in

image quality between scanners and imaging protocols. A future study involving various PET scanners from different vendors would better assess the robustness of the software and the VOI measurements. Furthermore, a prospective study in which raw listmode data were available would allow for investigation of optimal parameters in image acquisition, reconstruction, and analysis. In this study, for example, the VOI diameters for the vials and cold rods were selected to be half the actual diameters. The VOI dimensions affect noise versus accuracy, since a larger VOI means reduced noise from more statistical averaging but reduced accuracy from greater spillover at boundaries. The effect of scan time and image reconstruction parameters (voxel size, algorithm, number of iterations, postfiltering) on phantom quantitative measurements is another area further study.

Conclusion:

Automated software for analysis of ACR PET phantom images using 3D VOIs produces more consistent results compared to the current specified method, especially when normalizing for assayed syringe activities and dilution volumes used in phantom preparation. Quantitative assessment of high-contrast performance, low-contrast performance, SUV accuracy, and uniformity provides unbiased and meaningful evaluation of image quality. High accuracy of these quantitative measurements may allow for tighter acceptance ranges for PET scanner performance.

Disclosure:

No potential conflict of interest relevant to this article was reported.

References:

1. MacFarlane CR. ACR accreditation of nuclear medicine and PET imaging departments. *J Nucl Med Technol.* 2006;34:18-24.

2. American College of Radiology PET Accreditation Program: Testing Instructions. https://www.acraccreditation.org/-/media/ACRAccreditation/Documents/NucMed-PET/PET-Forms/PETPhantomInstructions.pdf?la=en. Updated November 19, 2018. Accessed December 4, 2018.

3. Madsen MT. A method for quantifying SPECT uniformity. *Med Phys.* 1997;24:1696-1700.

4. Lodge MA, Rahmim A, Wahl RL. Simultaneous measurement of noise and spatial resolution in PET phantom images. *Phys Med Biol.* 2010;55:1069-1081.

5. Wollenweber SD, Kemp BJ. Technical Note: Rod phantom analysis for comparison of PET detector sampling and reconstruction methods. *Med Phys.* 2016;43:6175.

6. Hirtl A, Bergmann H, Knausl B, Beyer T, Figl M, Hummel J. Technical Note: Fully-automated analysis of Jaszczak phantom measurements as part of routine SPECT quality control. *Med Phys.* 2017;44:1638-1645.

7. Ulrich EJ, Sunderland JJ, Smith BJ, et al. Automated model-based quantitative analysis of phantoms with spherical inserts in FDG PET scans. *Med Phys.* 2018;45:258-276.

8. Nichols KJ, DiFilippo FP, Palestro CJ. Texture analysis for automated evaluation of Jaszczak phantom SPECT system tests. *Med Phys.* 2018 [Epub ahead of print].

9. Makris NE, Huisman MC, Kinahan PE, Lammertsma AA, Boellaard R. Evaluation of strategies towards harmonization of FDG PET/CT studies in multicentre trials: comparison of scanner validation phantoms and data analysis procedures. *Eur J Nucl Med Mol Imaging.* 2013;40:1507-1515.

10. Grassroots DICOM. https://sourceforge.net/projects/gdcm/. Updated October 23, 2018. Accessed December 4, 2018.

11. Wells WM, 3rd, Viola P, Atsumi H, Nakajima S, Kikinis R. Multi-modal volume registration by maximization of mutual information. *Med Image Anal.* 1996;1:35-51.

12. Maes F, Collignon A, Vandermeulen D, Marchal G, Suetens P. Multimodality image registration by maximization of mutual information. *IEEE Trans Med Imaging.* 1997;16:187-198.

13. Coleman WP, Flynn TC, Coleman KM. When one liter does not equal 1000 milliliters: implications for the tumescent technique. *Dermatol Surg.* 2000;26:1024-1028.

14. Adams MC, Turkington TG, Wilson JM, Wong TZ. A systematic review of the factors affecting accuracy of SUV measurements. *AJR American journal of roentgenology.* 2010;195:310-320.

15. Lodge MA, Chaudhry MA, Wahl RL. Noise considerations for PET quantification using maximum and peak standardized uptake value. *J Nucl Med.* 2012;53:1041-1047.

16. Rahmim A, Qi J, Sossi V. Resolution modeling in PET imaging: Theory, practice, benefits, and pitfalls. *Med Phys.* 2013;40:064301.

17. Bai B, Bading J, Conti PS. Tumor Quantification in Clinical Positron Emission Tomography. *Theranostics.* 2013;3:787-801.

18. Lodge MA. Repeatability of SUV in Oncologic 18F-FDG PET. *J Nucl Med.* 2017;58:523-532.

19. DiFilippo FP. Technical Note: Automated quantitative analysis of planar scintigraphic resolution with the ACR SPECT phantom. *Med Phys.* 2018;45:1118-1122.

20. Cessna JT, Schultz MK, Leslie T, Bores N. Radionuclide calibrator measurements of (18)F in a 3ml plastic syringe. *Appl Radiat Isot.* 2008;66:988-993.

21. Zimmerman BE, Bergeron DE, Cessna JT. Impact of Recent Change in the National Institute of Standards and Technology Standard for 18F on the Relative Response of 68Ge-Based Mock Syringe Dose Calibrator Standards. *J Nucl Med.* 2015;56:1453-1457.

FIGURE 1. Example of standard quantitative measurements specified for ACR PET phantom evaluation. A transaxial slice of 10-mm thickness is generated which includes the hot and cold vials. Circular ROIs of 25-mm diameter are drawn, centered over each vial. A circular ROI (diameter between 60 mm and 70 mm) is drawn over the background region. Some pass/fail criteria are based on SUV measurements of these regions, while other pass/fail criteria depend on qualitative assessment of hot vial visibility, cold rods visibility, and background uniformity.

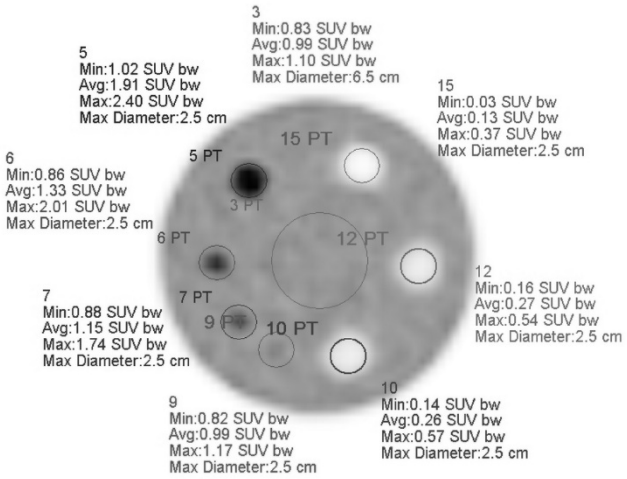

FIGURE 2. Histograms of SUV and normalized SUV measurements of the 16 mm hot vial for the 17 phantom studies. From left to right: SUV-max using the ACR ROI, SUV-vial using the cylindrical VOI, normalized SUV-max using the ACR ROI, and normalized SUV-vial using the cylindrical VOI. Most consistent results are obtained with the normalized SUV-vial measurements.

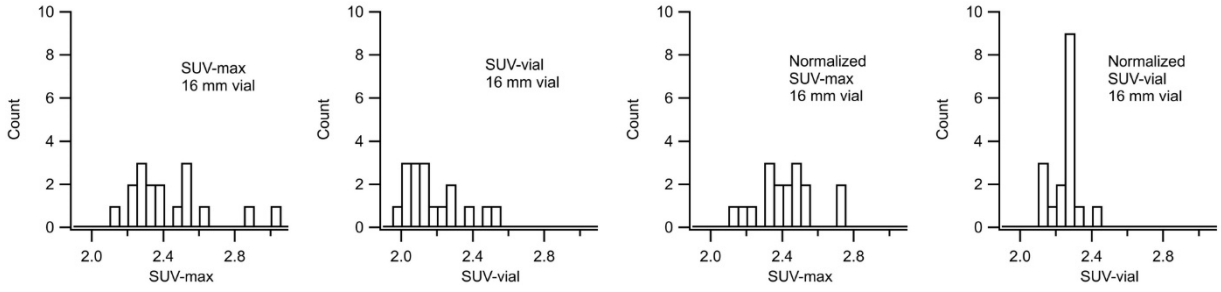

FIGURE 3. Histograms of SUV-max ratio (left) and SUV-vial ratio (right) for the 16 mm to 25 mm hot vials. The SUV-vial ratios were more consistent and, unlike the SUV-max ratios, did not have outliers greater than 1.0

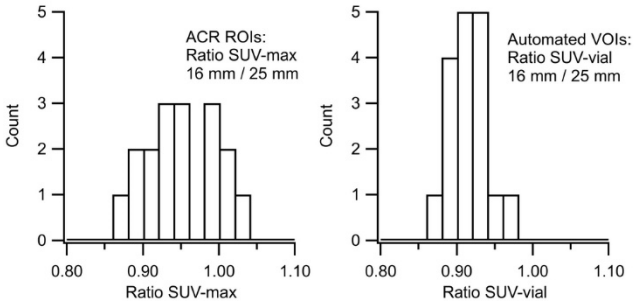

FIGURE 4. Cold rods contrast versus rod diameter (mean values for the 17 phantom studies analyzed). Standard deviation for each point is approximately 0.01; error bars are smaller than the size of the markers.

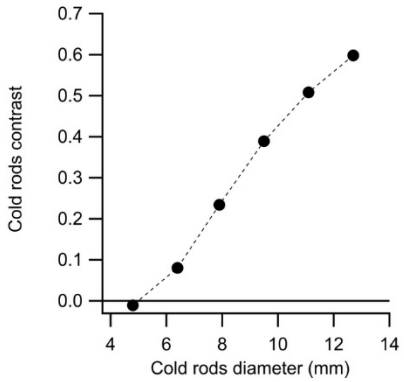

TABLE 1. Hot vial SUVs (mean ± percent standard deviation) measured according to ACR guidelines (SUV-max using 25 mm circular ROI in a 10 mm slice) and using the automated software (SUV-vial using cylindrical VOI). Normalized SUVs are also listed, which account for actual syringe activities and dilution vessel used during phantom preparation.

Hot vial diameter	ACR ROI SUV-max	Automated VOI SUV-vial	ACR ROI Normalized SUV-max	Automated VOI Normalized SUV-vial
25 mm	2.56 ± 6.7%	2.37 ± 6.2%	2.54 ± 3.6%	2.46 ± 3.1%
16 mm	2.43 ± 9.7%	2.16 ± 7.2%	2.41 ± 7.0%	2.24 ± 3.8%
12 mm	2.02 ± 6.0%	1.82 ± 5.6%	2.01 ± 5.2%	1.89 ± 2.4%
8 mm	1.35 ± 9.4%	1.29 ± 8.3%	1.34 ± 6.3%	1.34 ± 3.7%

TABLE 2. Hot vial SUV ratios (mean ± percent standard deviation) measured according to ACR guidelines (SUV-max using 25 mm circular ROI in a 10 mm slice) and using the automated software (SUV-vial using cylindrical VOI).

Hot vial ratio	ACR ROI SUV-max ratio	Automated VOI SUV-vial ratio
16 mm / 25 mm	0.95 ± 5.0%	0.91 ± 2.7%
12 mm / 25 mm	0.79 ± 6.7%	0.77 ± 3.3%
8 mm / 25 mm	0.53 ± 5.2%	0.54 ± 3.7%

TABLE 3. Cold rods contrast (mean value and standard deviation of the 17 studies) for the six sectors of the ACR PET phantom.

Rod diameter	12.7 mm	11.1 mm	9.5 mm	7.9 mm	6.4 mm	4.8 mm
Contrast (mean)	0.598	0.508	0.389	0.234	0.080	-0.011
Standard deviation	0.011	0.007	0.008	0.012	0.005	0.007